Biophysical *Journal*
Article

Biophysical Society

Intercellular Bridge Mediates Ca^{2+} Signals between Micropatterned Cells via IP_3 and Ca^{2+} Diffusion

Fulin Xing,[1] Songyue Qu,[1] Junfang Liu,[1] Jianyu Yang,[1] Fen Hu,[1] Irena Drevenšek-Olenik,[2] Leiting Pan,[1,*] and Jingjun Xu[1,3]

[1]The Key Laboratory of Weak-Light Nonlinear Photonics of Education Ministry, School of Physics and TEDA Institute of Applied Physics, Nankai University, Tianjin, China; [2]Faculty of Mathematics and Physics, University of Ljubljana, and J. Stefan Institute, Ljubljana, Slovenia; and [3]Collaborative Innovation Center of Extreme Optics, Shanxi University, Taiyuan, Shanxi, China

ABSTRACT Intercellular bridges are plasma continuities formed at the end of the cytokinesis process that facilitate intercellular mass transport between the two daughter cells. However, it remains largely unknown how the intercellular bridge mediates Ca^{2+} communication between postmitotic cells. In this work, we utilize BV-2 microglial cells planted on dumbbell-shaped micropatterned assemblies to resolve spatiotemporal characteristics of Ca^{2+} signal transfer over the intercellular bridges. With the use of such micropatterns, considerably longer and more regular intercellular bridges can be obtained than in conventional cell cultures. The initial Ca^{2+} signal is evoked by mechanical stimulation of one of the daughter cells. A considerable time delay is observed between the arrivals of passive Ca^{2+} diffusion and endogenous Ca^{2+} response in the intercellular-bridge-connected cell, indicating two different pathways of the Ca^{2+} communication. Extracellular Ca^{2+} and the paracrine pathway have practically no effect on the endogenous Ca^{2+} response, demonstrated by application of Ca^{2+}-free medium, exogenous ATP, and $P2Y_{13}$ receptor antagonist. In contrast, the endoplasmic reticulum Ca^{2+}-ATPase inhibitor thapsigargin and inositol trisphosphate (IP_3) receptor blocker 2-aminoethyl diphenylborate significantly inhibit the endogenous Ca^{2+} increase, which signifies involvement of IP_3-sensitive calcium store release. Notably, passive Ca^{2+} diffusion into the connected cell can clearly be detected when IP_3-sensitive calcium store release is abolished by 2-aminoethyl diphenylborate. Those observations prove that both passive Ca^{2+} diffusion and IP_3-mediated endogenous Ca^{2+} response contribute to the Ca^{2+} increase in intercellular-bridge-connected cells. Moreover, a simulation model agreed well with the experimental observations.

SIGNIFICANCE It is well proven that intercellular bridges formed at the end of the cytokinesis process facilitate intercellular mass transport between the daughter cells. However, their role in the mediation of Ca^{2+}-based intercellular communication between postmitotic cells is still largely unknown. In this work, we utilize BV-2 microglial cells planted on specially designed micropatterned assemblies to resolve the spatiotemporal characteristics of Ca^{2+} communication over the intercellular bridge. We show that both passive Ca^{2+} diffusion and inositol-triphosphate-mediated endogenous Ca^{2+} response contribute to the signal transfer.

INTRODUCTION

In most cell types at the end of the cytokinesis process, one cell divides into two daughter cells with formation of a transient intercellular bridge that connects the cells before their final separation (1–3). The formation of the intercellular bridge is driven by several consecutive steps, including cleavage furrow ingression, constriction of an actomyosin-based contractile ring, creation and stabilization of a connective microtubular linkage, and its final abscission (4,5). The majority of studies in this field are focused on molecular events associated with formation and abscission of the intercellular bridge such as assemblage of endosomal sorting complex required for transport III (ESCRT-III) (6–9) and localization of testis-expressed gene 14 (10,11). Recently, it was found that the intercellular bridge in the early mouse embryo served as the microtubule-organizing center and coordinated the transport of cell adhesion molecules to the membrane (12) and that stable intercellular bridges in germline cells facilitated the sharing of messenger RNA (13), organelles (14), and other molecules (15). However, more important functions and physical characteristics of intercellular bridges still remain largely unknown.

Submitted August 9, 2019, and accepted for publication January 6, 2020.

*Correspondence: plt@nankai.edu.cn

Editor: Heping Cheng.

https://doi.org/10.1016/j.bpj.2020.01.006

Ca^{2+} signaling is a principal form of cell-to-cell communication that coordinates the functions of a large group of cells and regulates various biological activities during growth and development (16–19). Ca^{2+} mobilization is triggered by the increase of cytoplasmic Ca^{2+} concentration in the initiating cell, which is subsequently followed by the increase of Ca^{2+} concentration in other cells. This process takes place either through the paracrine pathway in distant cells (20,21) or, in physically connected cells, through gap junction coupling (22,23). Regular gap junctions enable spreading of Ca^{2+} signals either directly, by diffusion of Ca^{2+} ions, or indirectly, by diffusion of messenger molecules such as inositol triphosphate (IP_3) (16,22,23). A recently discovered new type of cell-to-cell communication pathways, i.e., communication via tunneling nanotubes (TNTs) (24), was also reported to mediate the transmission of Ca^{2+} signals in multiple types of cells such as astrocytes (25), dendritic cells (26), and retinal pigment epithelial cells (27). As a physical continuity of the plasma between cells, TNTs represent a unique model to study Ca^{2+} signaling propagation in bounded narrow structures (28,29). Nevertheless, the instability and uncontrollability of TNTs restrict their suitability for advanced research on Ca^{2+} signaling.

In comparison to TNTs, intercellular bridges have larger width and exhibit better stability and controllability, which makes them an ideal system for quantitative analysis of Ca^{2+} signal propagation. In this work, we utilize BV-2 microglial cells to investigate the spatiotemporal characteristics of Ca^{2+} communication between postmitotic daughter cells via the intercellular bridge. The initial Ca^{2+} signal in one of the two daughter cells was provoked by a mechanical stimulus. A set of dumbbell-shaped micropatterned assemblies was used to regulate the length of the intercellular bridges formed during the cytokinesis. By this method, considerably longer and more regular intercellular bridges were obtained than in conventional cell cultures. A theoretical model mentioned above was used to simulate Ca^{2+} communication through the intercellular bridges, and very good agreement between experimental and computational results was found.

MATERIALS AND METHODS

Cell culture

The BV-2 microglial cells were routinely cultured in Dulbecco's modified Eagle's medium (Gibco, Gaithersburg, MD) containing 10% (v/v) fetal bovine serum (Biological Industries, Beit HaEmek, Israel), 100 U/mL penicillin, and 100 μg/mL streptomycin (Gibco) at 37°C under 5% CO_2. Before being planted on glass coverslips, cells were isolated with 0.25% trypsin (Gibco) and diluted to a density of 3×10^5 cells/mL.

Substrate preparation

The micropatterned substrates were fabricated as previously reported (30). First, clean glass coverslips were placed into a hermetic flask containing hexamethyldisilazane (HMDS; Sigma-Aldrich, St. Louis, MO) vapor to enable deposition for 20 min. Then, a positive photoresist (RuiHong, Suzhou City, China) was spun cast on HMDS-covered substrates and photoetched through a chrome-based photomask with designed patterns. After removing the exposed parts of the photoresist with a developing solution, the substrates were treated with oxygen plasma for 2 min and then dipped into anhydrous toluene containing 3 mM poly (ethylene glycol)-silane (Gelest, Morrisville, PA) and 1% (v/v) triethylamine (Sigma-Aldrich) for 3 days to attain stable passivation. Next, to remove polyethylene glycol attached to HMDS regions, the substrates were successively sonicated in anhydrous toluene, ethanol, and deionized water. Then, fibronectin (FN; Corning, Corning, NY) solution (150 μg/mL) in phosphate-buffered saline was spread over the substrates at 4°C for 20 min. Finally, the cell suspension (3×10^5 cells/mL) was planted on the substrates at 37°C for 20 min. After washing away the suspending cells with phosphate-buffered saline, the adherent cells were located on the designed patterns. The prepared cell assemblies were incubated at 37°C and 5% CO_2 for 2 h before the two-channel time-lapse snapping experiments or for 8 h before the Ca^{2+} imaging experiments.

For preparation of fluorescent FN, the FN solution was mixed with a reactive dye (Cy3.5; GE Healthcare, Amersham, UK) for 20 min. Then, the resulting Cy3.5-FN was spread onto the substrates. The Cy3.5-FN was excited by a mercury lamp with a 546/12 nm excitation filter, and the corresponding fluorescence emission was collected through a 590/35 nm emission filter.

Imaging

The fluorescence emission associated with calcium concentration in cytosol ($[Ca^{2+}]_c$) was detected by an electron multiplying charge-coupled device (DU-897D-CS0-BV; Andor, Belfast, UK) connected to an inverted fluorescent microscope (Axio Observer D1; Carl Zeiss, Oberkochen, Germany). The BV-2 microglial cells were loaded with 2 μM Fluo-4 AM (Invitrogen, Carlsbad, CA) in Hank's balanced salt solution (137 mM NaCl, 5.3 mM KCl, 2 mM $CaCl_2$, 1 mM $MgCl_2$, 5.5 mM glucose, 10 mM HEPES (pH 7.4)) for 30 min at 37°C. After bathing in Hank's balanced salt solution for 10 min, they were excited by a mercury lamp using a 485/0 nm excitation filter. The fluorescence emission was collected by a 40×/1.30 oil objective with a 540/50 nm emission filter. The acquired images were analyzed by MetaMorph software (Molecular Devices, San Jose, CA). Changes of $[Ca^{2+}]_c$ are presented by modifications of the relative fluorescence intensity F/F_0 (intensity after stimulation/basal intensity before stimulation).

A two-channel time-lapse imaging was performed by using an inverted fluorescent microscope (Ti-E; Nikon, Tokyo, Japan) combined with a CCD (Retiga R1; Qimaging, Surrey, Canada) detector. The images were acquired with Micro-Manager software (National Institutes of Health, Bethesda, MD) at a rate of 1 frame every 3 min.

Mechanical stimulus

A glass microelectrode with a 1-μm-diameter tip fixed on a Three-axis Hanging Joystick Oil Hydraulic Micromanipulator (MMO-202ND; Narishige, Tokyo, Japan) was used to mechanically stimulate single BV-2 microglial cells. The tip was manipulated to provoke a gentle stimulation on the membrane of a selected micropatterned cell.

Statistical analysis

When a selected cell exhibited a rise of $[Ca^{2+}]_c$ resulting in $(F_{max}/F_0) > 1.1$, it was regarded as a Ca^{2+}-responsive cell. The response ratio is defined as the number of responsive intercellular-bridge-connected cells divided by the total number of all intercellular-bridge-connected cells in the investigated group. The response intensity is defined as the fluorescence intensity of the Ca^{2+} signal in the stimulated state divided by the fluorescence intensity in the resting state. The length of the intercellular bridge is defined as the length of the connecting tissue that has a width of less than 2 μm. The abscission time is defined

as the time interval between the moment at which the cell was divided into two cells and the moment at which the intercellular bridge was terminated. The obtained data are presented as the mean ± standard deviation (SD). For statistical comparison between different groups, the data were analyzed by GraphPad Prism software (version 6) using an unpaired Student's *t*-test. The values of $p < 0.05$ were considered to be statistically significant.

RESULTS

Propagation of Ca^{2+} waves between BV-2 microglial cells connected with intercellular bridges

First, BV-2 microglial cells cultured on traditional substrates were investigated. They formed intercellular bridges during the cell division (Fig. 1 *A*). The immunostaining experiment demonstrated that the intercellular bridges were composed of microtubular bundles with a characteristic midbody structure located in the middle of the intercellular bridge (Fig. S1 *A*). Although some intercellular bridges were as long as 30 μm, most of them were shorter than 5 μm (Fig. S1 *B*). Before applying the mechanical stimulus (Fig. 1 *A*), all cells were in the resting state according to the stable basal $[Ca^{2+}]_c$ ($F/F_0 = 1$ in Fig. 1 *B*). As can be seen in Fig. 1 and Video S1, a gentle touch of the microelectrode evoked a rapid increase of $[Ca^{2+}]_c$ in cell 1, followed by propagation of the signal through the intercellular bridge and mobilization of $[Ca^{2+}]_c$ in the body of cell 2. This observation demonstrates that intercellular bridges are capable of mediating Ca^{2+} communication. Interestingly, cell 3, which was physically separated from cells 1 and 2, also exhibited an increase of $[Ca^{2+}]_c$. This increase was stimulated through the paracrine pathway. As demonstrated in our previous work, the transmitters mediating the Ca^{2+} communication are secreted from the stimulated site of the cell (30). Therefore, the secreting site on cell 1 (marked by an *asterisk* in Fig. 1 *A*) was almost equidistant from cell 2 and cell 3, whereas the increase of $[Ca^{2+}]_c$ in cell 2 appeared much faster than in cell 3 (Fig. 1 *B*). This result suggests that Ca^{2+} communication mediated by the intercellular bridge is considerably faster than Ca^{2+} communication mediated by the paracrine pathway.

To resolve additional details on the spatiotemporal characteristics of the Ca^{2+} communication mediated by the intercellular bridge, we developed a simple micropatterning strategy to induce longer intercellular bridges. This strategy was motivated by the expectation that measurements of Ca^{2+} propagation velocities would be more precise on longer intercellular bridges. Moreover, with a predesigned bridging location, the mechanical stimulus can be always applied at one and the same site of the stimulated cells.

Regulation of intercellular bridges with micropatterned assemblies

To induce longer intercellular bridges between BV-2 microglial cells, we designed a set of dumbbell-shaped micropatterns. Circular parts of the patterns had a diameter of 18 μm (Fig. 2 *A*), which corresponds to the typical size of BV-2 microglial cells cultured on traditional substrates. A bar connecting the two circular ends had a width of 6 μm and lengths in the range from 2 to 30 μm. The fluorescence distribution of Cy3.5-FN deposited onto such a pattern is also shown in Fig. 2 *A* and reveals that the FN area is consistent with the designed pattern. When single BV-2 microglial cells were cultured on the substrates, they adhered to one of the two circular regions, as shown in Fig. 2 *B*. Then, the cell divided into two daughter cells that moved away from each other and formed an intercellular bridge between them. The bridge was located on top of the connecting bar of the dumbbell-shaped micropattern (Fig. 2 *B*; Video S2). To select optimal micropatterns for the following Ca^{2+} imaging experiments, we performed statistical analysis of the maximal observed length (before final abscission) of the intercellular

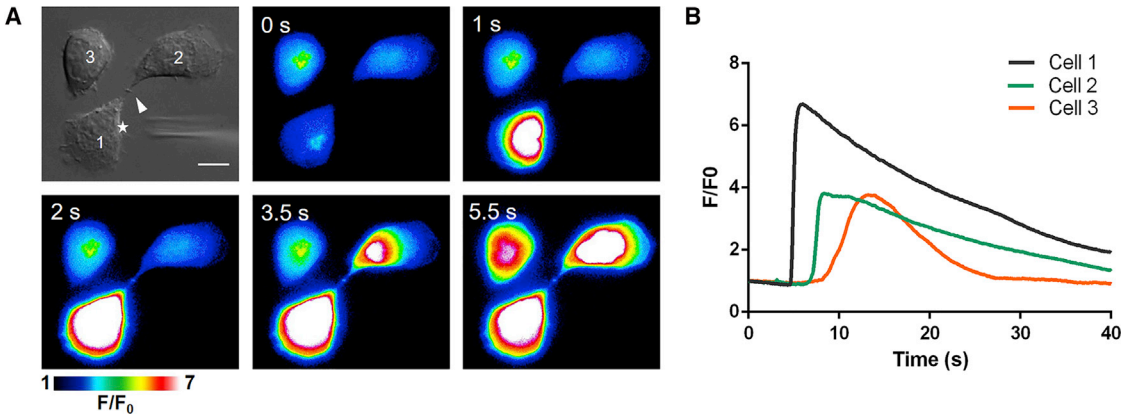

FIGURE 1 Ca^{2+} communication among BV-2 microglial cells. (*A*) A sequential series of pseudocolor fluorescence images of Ca^{2+} communication between the cells is given. The signal was elicited by a mechanical stimulus (glass electrode) applied to cell 1. The asterisk indicates the stimulated site. Cells 1 and 2 are connected with an intercellular bridge. The white arrow indicates the location of the midbody of the intercellular bridge. Scale bar, 10 μm. (*B*) The $[Ca^{2+}]_c$ traces of the three cells shown in (*A*) are shown. The Ca^{2+} mobilization in cell 2 is significantly faster than in cell 3. To see this figure in color, go online.

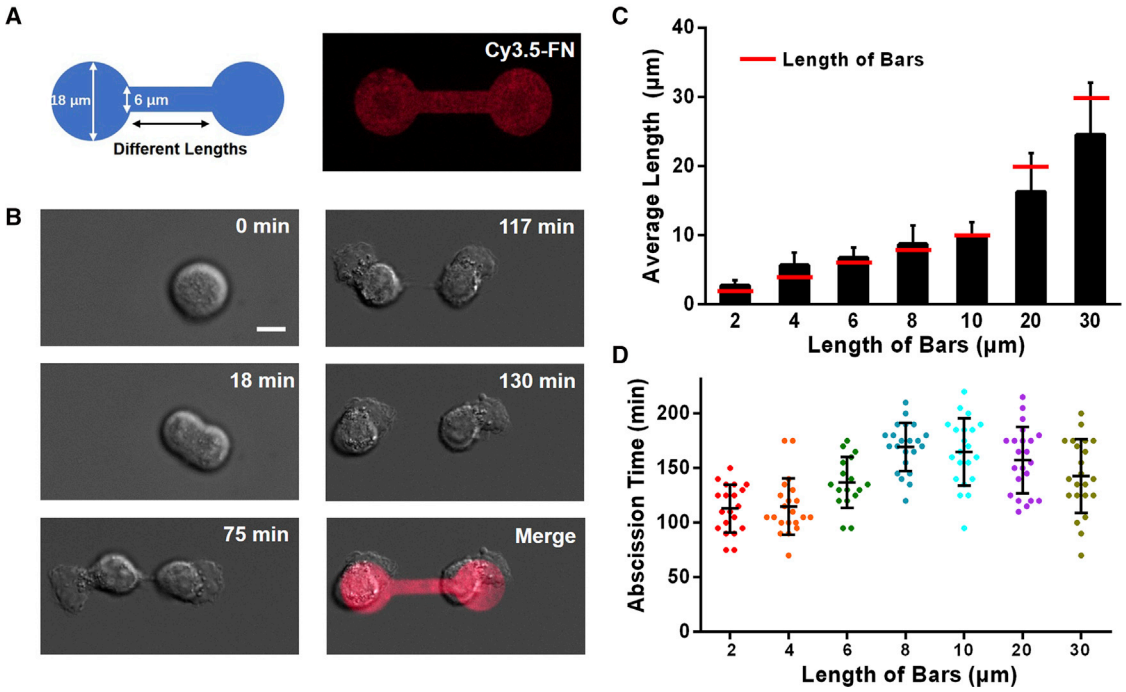

FIGURE 2 Formation of intercellular bridge between BV-2 microglial cells adhered to a dumbbell-shaped micropattern. (*A*) The designed shape (*left*) and the corresponding fluorescence image of Cy3.5-FN bound to HMDS-covered regions (*right*) are shown. (*B*) The daughter BV-2 microglial cells form an intercellular bridge between them. Scale bar, 10 μm. (*C*) Maximal observed lengths of intercellular bridges formed on the patterns with connecting bars of different lengths are shown. The red lines designate the length of the bars. (*D*) Abscission time of the intercellular bridges formed on the patterns with connecting bars of different lengths is shown. Horizontal lines indicate mean ± SD. To see this figure in color, go online.

bridge as a function of the length of the connecting bar. As shown in Fig. 2 *C*, the lengths of intercellular bridges were 2.7 ± 0.8, 5.7 ± 1.8, 6.7 ± 1.5, 8.7 ± 2.7, 9.8 ± 2.2, 16.3 ± 5.6, and 24.5 ± 7.8 μm for the bars with lengths of 2, 4, 6, 8, 10, 20, and 30 μm, respectively. One can notice that for bars shorter than 10 μm, the average length of the resultant intercellular bridges is longer than the length of the bars, whereas for bars longer than 10 μm, it is shorter. Fig. 2 *D* shows the corresponding values of the abscission times, which are 113 ± 22, 115 ± 26, 137 ± 23, 169 ± 22, 165 ± 31, 157 ± 31, and 143 ± 34 min. In general, the abscission time increases with increasing length, indicating that longer intercellular bridges are more stable than the short ones. In according with this finding, we chose a pattern with bar lengths of 8, 10, 20, and 30 μm for further experiments. We also found that the response ratios and the response intensities decreased slightly as the bar lengths of the pattern increased from 8 to 30 μm (Fig. S2). This might be because longer intercellular bridges are often narrower, which impedes intercellular transmission.

Passive Ca^{2+} diffusion and endogenous Ca^{2+} response contribute to increase of $[Ca^{2+}]_c$ in the connected cell

We recorded modifications of $[Ca^{2+}]_c$ as a function of time after mechanical stimulation of one of the two connected cells. A typical result presented in the form of a kymograph image is shown in Fig. 3 *A* (see also Video S3). The cell on the right side was stimulated first. Afterwards, a weak passive Ca^{2+} diffusion propagating from the stimulated cell to the midbody of the intercellular bridge and then to the opposite end of the bridge was detected. The evolution of this signal is indicated in Fig. 3 *A* by the dashed line K2. Then, an endogenous Ca^{2+} response took place in the connected cell (Fig. 3 *A*; Video S3). The corresponding signal was much larger than the signal from passive Ca^{2+} diffusion and emanated from the central part of the cell body of connected cell rather than from the joint between the connected cell and the intercellular bridge. This observation indicates an indirect pathway of the $[Ca^{2+}]_c$ increase in the connected cell. The evolution of this signal is indicated in Fig. 3 *A* by the dashed line K1. Quantitative statistical analysis of the slopes of K1 and K2 is presented in Fig. 3 *B*. The slope of K2 (9.7 ± 2.7 μm/s) corresponds to an effective transit velocity of passive Ca^{2+} diffusion along the intercellular bridge. The slope of K1 (6.6 ± 2.0 μm/s) corresponds to an effective propagation velocity of the endogenous Ca^{2+} signal. From those observations it follows that both passive Ca^{2+} diffusion and endogenous Ca^{2+} response contribute to the increase of $[Ca^{2+}]_c$ in intercellular-bridge-connected cells. The former is faster but quite weak, whereas the latter is slower but much stronger.

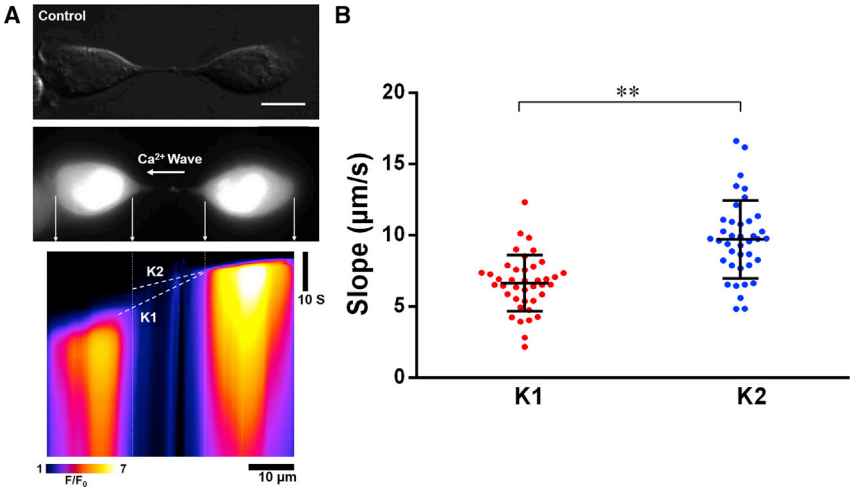

FIGURE 3 Time dependence of Ca^{2+} communication between intercellular-bridge-connected cells adhered to the dumbbell-shaped micropattern. (*A*) A linescan of the Ca^{2+} fluorescence along the intercellular bridge on a 10-μm-long bar is shown. The dashed line K1 connects the end of the intercellular bridge on the stimulated cell with the initiating point of endogenous Ca^{2+} response in the connected cell. The dashed line K2 is drawn along the Ca^{2+} diffusion signal observed in the intercellular bridge. Scale bars, 10 μm. (*B*) The slopes of K1 and K2 in (*A*) are shown. $^{**}p < 0.001$, comparing with K1. Horizontal lines indicate mean $\pm$ SD. To see this figure in color, go online.

Transmission of IP_3 via intercellular bridge mediates endogenous Ca^{2+} response in the connected cell

To elucidate the source of endogenous Ca^{2+} response, various reagents were applied to the cells before mechanical stimulation. Fig. 4 shows the corresponding response ratios and response intensities of the associated endogenous Ca^{2+} signal. The results show Ca^{2+}-free medium treatment had no impact on signal propagation, indicating its independence from extracellular Ca^{2+}. Our previous work showed that pretreatment with ATP (10 μM) could terminate Ca^{2+} communication mediated by the paracrine (30,31). In this work, pretreatment with 10 μM ATP had almost no effect, which indicates that for intercellular-bridge-mediated Ca^{2+} communication, the paracrine pathway is practically negligible. Moreover, a similar result was obtained when cells were pretreated with MRS 2211 (10 μM, 15 min), a $P2Y_{13}$ receptor-specific inhibitor that could block the paracrine-mediated intercellular Ca^{2+} communication in BV-2 microglia (31).

The cells were also pretreated with application of endoplasmic reticulum Ca^{2+}-ATPase inhibitor thapsigargin (TG) (32) and IP_3 receptor blocker 2-aminoethyl diphenylborate (2-APB) (33). The preincubation took place for 10 min at room temperature with either 2 μM TG or with 15 μM 2-APB. Both of those reagents significantly decreased the response ratios (Fig. 4 *A*) and the response intensities (Fig. 4 *B*) of Ca^{2+} in the connected cell, suggesting that the main source of intercellular-bridge-mediated endogenous Ca^{2+} response is IP_3-sensitive calcium store release.

In contrast to endogenous Ca^{2+} response, passive Ca^{2+} diffusion into the connected cells was clearly observed even when the endogenous Ca^{2+} response was inhibited by the 2-APB (*arrows* in Fig. 5 *A*; Video S4). In this case, a slight increase of Ca^{2+} fluorescence initiated from the end of the intercellular bridge was detected without a subsequent endogenous Ca^{2+} response in the central part of the connected cell. The traces represented in Fig. 5 *B* show that Ca^{2+} flowed into the intercellular bridge practically immediately after the $[Ca^{2+}]_c$ increase in the stimulated cell, whereas a significantly weaker Ca^{2+} increase occurred in the connected cell. On the other hand, we applied BAPTA-AM (10 μM, 20 min), a potent free Ca^{2+} chelator, to further study intercellular bridge-mediated Ca^{2+} signals. The results showed that Ca^{2+} diffusion fluorescence was completely suppressed, whereas IP_3-mediated Ca^{2+} release

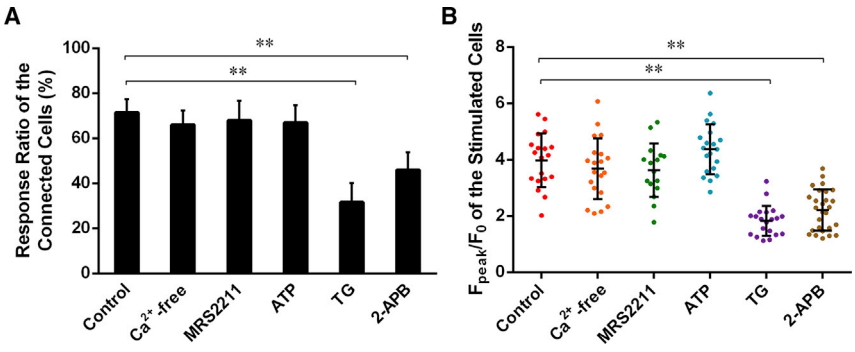

FIGURE 4 Ca^{2+} response of intercellular-bridge-connected BV-2 microglial cells after drug treatment. (*A*) Response ratios of the Ca^{2+} signal in intercellular-bridge-connected BV-2 microglial cells after treatment with different reagents are shown. $^{**}p < 0.001$; compare with the control group. (*B*) Response intensities of the Ca^{2+} signal in intercellular-bridge-connected BV-2 microglial cells after treatment with the same reagents as in (*A*) are shown. $^{**}p < 0.001$; compare with the control group. Horizontal lines indicate mean $\pm$ SD. At minimum, 20 cells were counted in each group. To see this figure in color, go online.

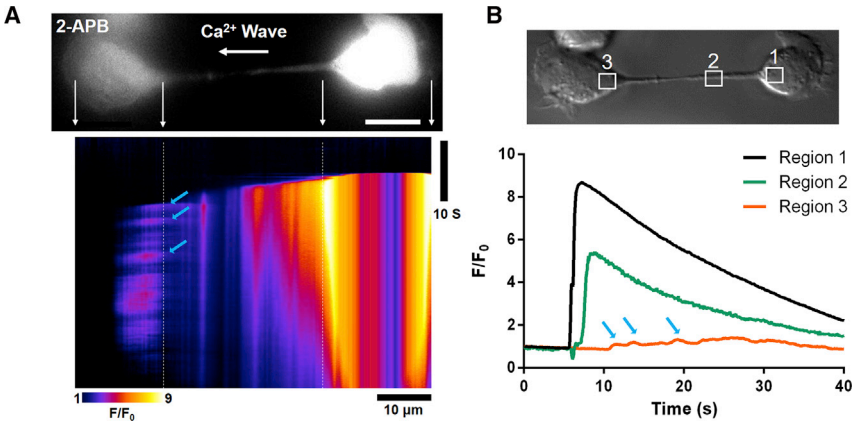

FIGURE 5 Ca^{2+} communication between intercellular-bridge-connected cells on the dumbbell-like micropattern after 2-APB treatment. (*A*) A line-scan of Ca^{2+} fluorescence along the intercellular bridge of two dumbbell-shaped micropattern-adhered cells exposed to 2-APB pretreatment on a 20 μm bar is shown. Scale bars, 10 μm. (*B*) Temporal traces of $[Ca^{2+}]_c$ detected in three different regions marked as 1, 2, and 3 are shown. The blue arrows indicate the Ca^{2+} flow into the connected cell positioned on the left side in (*A*). To see this figure in color, go online.

fluorescence just decreased evidently (Fig. S3; Video S5). The Ca^{2+} dissociation constants are ~345 and ~700 nM for fluo-4 (34) and BAPTA (35), respectively, suggesting that BAPTA binds free Ca^{2+} more easily than fluo-4. Thus, the large majority of the released Ca^{2+} was chelated by BAPTA after IP_3 activated calcium stores in the connected cell, which resulted in a small increase of Ca^{2+} fluorescence (*orange line* in Fig. S3 *B*). Meanwhile, the Ca^{2+} diffusion fluorescence through the intercellular bridge was totally blocked because of the BAPTA chelation (*green line* in Fig. S3 *B*). According to these results, we believe that intercellular communication via direct Ca^{2+} diffusion is also important for cell-cell communication between intercellular-bridge-connected cells.

Simulation of Ca^{2+} and IP_3 diffusion through the intercellular bridge

To verify the possibility that passive Ca^{2+} diffusion along the intercellular bridge can increase $[Ca^{2+}]_c$ level in the connected cell, we simulated Ca^{2+} diffusion between two cells connected by intercellular bridges using the model previously described (28) (Supporting Materials and Methods). Results show that passive diffusion of Ca^{2+} raises calcium concentration in the intercellular bridge ($[Ca^{2+}]_b$) (Fig. 6 *A*) as well as in the connected cell ($[Ca^{2+}]_c$) (Fig. 6 *B*), in good accordance with the experimental results shown in Fig. 5.

Previous work reported that Ca^{2+} diffusion in cytoplasm was much slower than IP_3 diffusion because Ca^{2+} buffer in cytoplasm could bind to Ca^{2+} ions and slow their motion (36). However, in our system, the IP_3-mediated Ca^{2+} response in the connected cell was slower than the passive Ca^{2+}-diffusion-mediated response (Fig. 3). After the application of mechanical stimulus, the concentrations of both Ca^{2+} and of IP_3 increased in the stimulated cell. Subsequently, their diffusion through the intercellular bridge toward the connected cell took place. As reported in (37,38), IP_3 in the connected cell should reach a threshold concentration of ~0.5 μM to be able to induce an endogenous Ca^{2+} release. As can be seen in Fig. 6 *D*, in our system, this causes a delay of some seconds, which in our opinion explains why in intercellular-bridge-connected cells, endogenous Ca^{2+}-response-based signaling is slower than passive Ca^{2+}-diffusion-based signaling.

DISCUSSION

The increase of Ca^{2+} level in cytosol plays a crucial role in various processes during cell division such as activation of Aurora-A kinase at mitosis (39), modulation of spindle formation and the onset of anaphase (40), and induction of calmodulin-dependent protein kinase II, which triggers the exit from meiosis (41). Our results clearly demonstrate that intercellular bridges mediate the cytosol Ca^{2+} levels via two different pathways, which brings a new perspective to the general understanding of Ca^{2+} regulation during mitosis.

TNTs, a tube-like continuity in plasma membrane and cytoplasm of adjacent cells, are formed by protrusion of filopodia or the separation of contacted cells with a length of tens of micrometers and a width of 50–200 nm (42). They allow intercellular transmission of multiple types of cellular components such as proteins, RNAs, viruses, and organelles (43,44). It has been established how TNTs facilitate Ca^{2+} signaling between isolated cells and that the diffusion of IP_3 along the TNTs and IP_3-mediated Ca^{2+} liberation promote the propagation of Ca^{2+} signals through them (28,29). Our observations indicate that, similar to TNTs, intercellular bridges also predominantly facilitate the IP_3-mediated Ca^{2+} liberation. However, because intercellular bridges are relatively wide in comparison to TNTs, passive diffusion of Ca^{2+} through them can also induce the raise of $[Ca^{2+}]_c$ in the connected cells. In accordance with that assumption, we carried out numerical simulations by using a model developed for TNTs (28) but considering a larger radius (~1 μm instead of ~200 nm) of the connecting tubes. The obtained results are in good

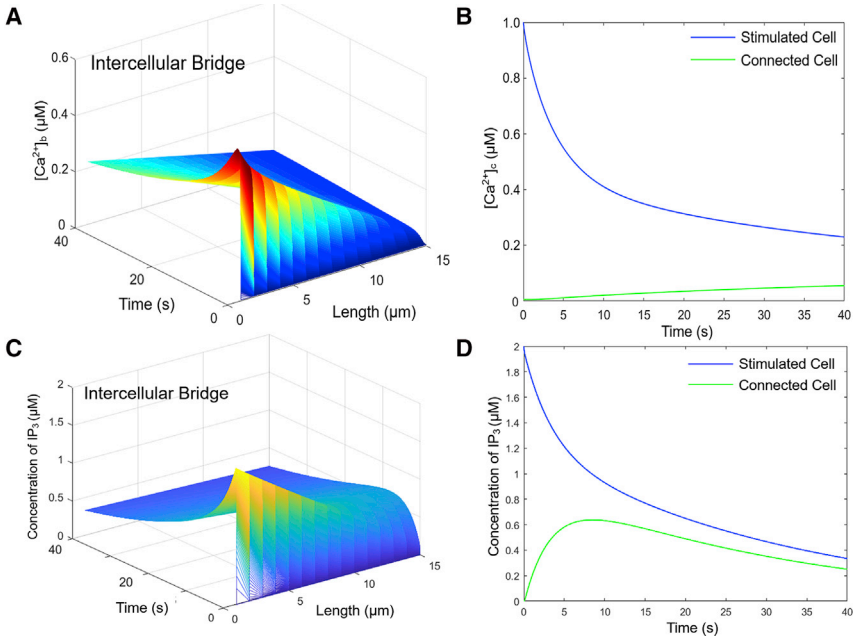

FIGURE 6 Simulated concentrations of Ca^{2+} and IP_3 progressing from the stimulated to the connected cell through the intercellular bridge. (*A*) Time dependencies of concentration of Ca^{2+} (after mechanical stimulus) at different positions of the intercellular bridge are shown. (*B*) Time dependencies of concentration of Ca^{2+} in stimulated and in connected cells are shown. (*C*) Time dependencies of concentration of IP_3 (after mechanical stimulus) at different positions of the intercellular bridge are shown. (*D*) Time dependencies of concentration of IP_3 in stimulated and in connected cells are shown. To see this figure in color, go online.

accordance with experimental observations. Another intercellular linkage, gap junction channels, are composed of two end-to-end hemichannels, each of which contains six connexin subunits surrounding the central pore (~40 Å in diameter) (45). Gap junctions can also mediate communication between closely contacted cells by facilitating the exchange of small molecules and ions (46). It has been reported that gap junctions mediate the intercellular Ca^{2+} signaling through the diffusion of Ca^{2+} and IP_3-mediated Ca^{2+} release (47), which is similar to our results on the intercellular-bridge-mediated Ca^{2+} communication.

Our work also provides an appealing demonstration of the versatility of micropatterning as an emerging powerful tool for single-cell control. Recently, micropatterning techniques have been successfully used in investigations of diverse biological processes such as cellular communication (48,49), migration (50,51), and cell proliferation and differentiation (52,53). Our previous study with ring-shaped micropatterned cell assemblies provided experimental evidence of a regenerative amplification mechanism that mediates Ca^{2+} communication between physically isolated BV-2 microglial cells via the paracrine pathway (30). In this study, dumbbell-shaped micropatterns are used as adhesive islands for control and lengthening of the intercellular bridges between connected cells.

We observed that the abscission time of the intercellular bridge was longer for longer bars. Lafaurie-Janvore et al. obtained a similar result for HeLa cells by using disk-shaped and bar-shaped patterns (7). They further proved that lengthening of the intercellular bridge prevented the assembly of ESCRT-III, which resulted in delayed abscission. When tension along the bridge was released, ESCRT-III assembled and induced membrane fission, followed by abscission. This may also explain why in our experiments, long intercellular bridges have longer lifetimes than shorter ones.

Recently, a cell-cycle-dependent mitochondrial Ca^{2+} transient was found to coordinate energy production in mitochondria and promote mitotic progression (54). Mitochondria are known to be important sensors, stores, and regulators of Ca^{2+} (55,56). Interestingly, in our experiments, by using Mito-Tracker Orange we also observed mitochondria resident in intercellular bridges between the BV-2 microglial cells (Fig. S4). Therefore, we suspect that mitochondria acting as regenerative amplifiers may facilitate also the propagation of Ca^{2+} waves over the intercellular bridges. Thus, Ca^{2+} communication mediated by intercellular bridges may regulate formation and abscission processes of cytokinesis through the interaction with mitochondria. Further experiments are needed to analyze the correlation between different processes and verify this proposition.

In summary, we induced long intercellular bridges between BV-2 microglial cells using dumbbell-like micropatterns, by which the spatiotemporal characteristics of mechanical-stimulus-evoked Ca^{2+} communication through the intercellular bridge were resolved. Ca^{2+} in the intercellular bridge was observed to transit faster than the responding velocity between intercellular bridge-connected cells. Our results using TG and 2-APB demonstrated that the main source of $[Ca^{2+}]_c$ increase in connected cell was passive Ca^{2+} diffusion and IP_3-sensitive calcium store release. A theoretical simulation also confirmed the experimental observations. Our work brings a new understanding of Ca^{2+} signaling mediated by the intercellular bridge during mitosis, as well as proposing an insight into the Ca^{2+} transmission in narrow bounded structures.

SUPPORTING MATERIAL

Supporting Material can be found online at https://doi.org/10.1016/j.bpj.2020.01.006.

AUTHOR CONTRIBUTIONS

F.X., J.L., and J.Y. performed the experiments. F.X. and S.Q. performed the simulations. F.X. and F.H. analyzed the data. L.P., F.X., and I.D.-O. wrote the article. L.P. and J.X. designed and supervised the work.

ACKNOWLEDGMENTS

This work was supported by the National Natural Science Foundation of China (no. 11574165, 11874231, and 31801134), Tianjin Natural Science Foundation (no. 18JCQNJC02000), the PCSIRT (Program for Changjiang Scholars and Innovative Research Team in University, no. IRT_13R29), the 111 Project (no. B07013), and Slovenian Research Agency (ARRS, research program P1-0192 and project of bilateral cooperation between Slovenia and China BI-CN/17-18-018).

REFERENCES

1. Lacroix, B., and A. S. Maddox. 2012. Cytokinesis, ploidy and aneuploidy. *J. Pathol.* 226:338–351.
2. Burton, K., and D. L. Taylor. 1997. Traction forces of cytokinesis measured with optically modified elastic substrata. *Nature.* 385:450–454.
3. Kechad, A., S. Jananji, …, G. R. X. Hickson. 2012. Anillin acts as a bifunctional linker coordinating midbody ring biogenesis during cytokinesis. *Curr. Biol.* 22:197–203.
4. Gromley, A., C. Yeaman, …, S. J. Doxsey. 2005. Centriolin anchoring of exocyst and SNARE complexes at the midbody is required for secretory-vesicle-mediated abscission. *Cell.* 123:75–87.
5. Steigemann, P., and D. W. Gerlich. 2009. Cytokinetic abscission: cellular dynamics at the midbody. *Trends Cell Biol.* 19:606–616.
6. Fededa, J. P., and D. W. Gerlich. 2012. Molecular control of animal cell cytokinesis. *Nat. Cell Biol.* 14:440–447.
7. Lafaurie-Janvore, J., P. Maiuri, …, M. Piel. 2013. ESCRT-III assembly and cytokinetic abscission are induced by tension release in the intercellular bridge. *Science.* 339:1625–1629.
8. Guizetti, J., L. Schermelleh, …, D. W. Gerlich. 2011. Cortical constriction during abscission involves helices of ESCRT-III-dependent filaments. *Science.* 331:1616–1620.
9. Goliand, I., S. Adar-Levor, …, N. Elia. 2018. Resolving ESCRT-III spirals at the intercellular bridge of dividing cells using 3D STORM. *Cell Rep.* 24:1756–1764.
10. Greenbaum, M. P., W. Yan, …, M. M. Matzuk. 2006. TEX14 is essential for intercellular bridges and fertility in male mice. *Proc. Natl. Acad. Sci. USA.* 103:4982–4987.
11. Greenbaum, M. P., N. Iwamori, …, M. M. Matzuk. 2009. Mouse TEX14 is required for embryonic germ cell intercellular bridges but not female fertility. *Biol. Reprod.* 80:449–457.
12. Zenker, J., M. D. White, …, N. Plachta. 2017. A microtubule-organizing center directing intracellular transport in the early mouse embryo. *Science.* 357:925–928.
13. Guo, G. Q., and G. C. Zheng. 2004. Hypotheses for the functions of intercellular bridges in male germ cell development and its cellular mechanisms. *J. Theor. Biol.* 229:139–146.
14. Ventelä, S., J. Toppari, and M. Parvinen. 2003. Intercellular organelle traffic through cytoplasmic bridges in early spermatids of the rat: mechanisms of haploid gene product sharing. *Mol. Biol. Cell.* 14:2768–2780.
15. Schulze, E. S., and S. H. Blose. 1984. Passage of molecules across the intercellular bridge between post-mitotic daughter cells. *Exp. Cell Res.* 151:367–373.
16. Leybaert, L., and M. J. Sanderson. 2012. Intercellular Ca($^{2+}$) waves: mechanisms and function. *Physiol. Rev.* 92:1359–1392.
17. Hao, M. M., A. J. Bergner, …, H. M. Young. 2017. Spontaneous calcium waves in the developing enteric nervous system. *Dev. Biol.* 428:74–87.
18. Sung, Y. J., Z. Sung, …, C. H. Lin. 2003. Intercellular calcium waves mediate preferential cell growth toward the wound edge in polarized hepatic cells. *Exp. Cell Res.* 287:209–218.
19. Guan, C. B., H. T. Xu, …, M. M. Poo. 2007. Long-range Ca^{2+} signaling from growth cone to soma mediates reversal of neuronal migration induced by slit-2. *Cell.* 129:385–395.
20. Arcuino, G., J. H.-C. Lin, …, M. Nedergaard. 2002. Intercellular calcium signaling mediated by point-source burst release of ATP. *Proc. Natl. Acad. Sci. USA.* 99:9840–9845.
21. Wang, N., M. De Bock, …, L. Leybaert. 2013. Paracrine signaling through plasma membrane hemichannels. *Biochim. Biophys. Acta.* 1828:35–50.
22. Jørgensen, N. R., S. C. Teilmann, …, T. H. Steinberg. 2003. Activation of L-type calcium channels is required for gap junction-mediated intercellular calcium signaling in osteoblastic cells. *J. Biol. Chem.* 278:4082–4086.
23. Suadicani, S. O., C. E. Flores, …, E. Scemes. 2004. Gap junction channels coordinate the propagation of intercellular Ca^{2+} signals generated by P2Y receptor activation. *Glia.* 48:217–229.
24. Rustom, A., R. Saffrich, …, H. H. Gerdes. 2004. Nanotubular highways for intercellular organelle transport. *Science.* 303:1007–1010.
25. Wang, X., N. V. Bukoreshtliev, and H. H. Gerdes. 2012. Developing neurons form transient nanotubes facilitating electrical coupling and calcium signaling with distant astrocytes. *PLoS One.* 7:e47429.
26. Watkins, S. C., and R. D. Salter. 2005. Functional connectivity between immune cells mediated by tunneling nanotubules. *Immunity.* 23:309–318.
27. Wittig, D., X. Wang, …, C. Roehlecke. 2012. Multi-level communication of human retinal pigment epithelial cells via tunneling nanotubes. *PLoS One.* 7:e33195.
28. Smith, I. F., J. Shuai, and I. Parker. 2011. Active generation and propagation of Ca^{2+} signals within tunneling membrane nanotubes. *Biophys. J.* 100:L37–L39.
29. Lock, J. T., I. Parker, and I. F. Smith. 2016. Communication of Ca($^{2+}$) signals via tunneling membrane nanotubes is mediated by transmission of inositol trisphosphate through gap junctions. *Cell Calcium.* 60:266–272.
30. Xing, F., P. Zhang, …, J. Xu. 2018. Spatiotemporal characteristics of intercellular calcium wave communication in micropatterned assemblies of single cells. *ACS Appl. Mater. Interfaces.* 10:2937–2945.
31. Jiang, P., F. Xing, …, J. Xu. 2017. Nucleotide transmitters ATP and ADP mediate intercellular calcium wave communication via $P2Y_{12/13}$ receptors among BV-2 microglia. *PLoS One.* 12:e0183114.
32. Thastrup, O., P. J. Cullen, …, A. P. Dawson. 1990. Thapsigargin, a tumor promoter, discharges intracellular Ca^{2+} stores by specific inhibition of the endoplasmic reticulum $Ca^{2(+)}$-ATPase. *Proc. Natl. Acad. Sci. USA.* 87:2466–2470.
33. Gregory, R. B., G. Rychkov, and G. J. Barritt. 2001. Evidence that 2-aminoethyl diphenylborate is a novel inhibitor of store-operated Ca^{2+} channels in liver cells, and acts through a mechanism which does not involve inositol trisphosphate receptors. *Biochem. J.* 354:285–290.
34. Gee, K. R., K. A. Brown, …, I. Johnson. 2000. Chemical and physiological characterization of fluo-4 Ca($^{2+}$)-indicator dyes. *Cell Calcium.* 27:97–106.
35. Pethig, R., M. Kuhn, …, L. F. Jaffe. 1989. On the dissociation constants of BAPTA-type calcium buffers. *Cell Calcium.* 10:491–498.

36. Wagner, J., and J. Keizer. 1994. Effects of rapid buffers on Ca^{2+} diffusion and Ca^{2+} oscillations. *Biophys. J.* 67:447–456.

37. Lemon, G., W. G. Gibson, and M. R. Bennett. 2003. Metabotropic receptor activation, desensitization and sequestration-I: modelling calcium and inositol 1,4,5-trisphosphate dynamics following receptor activation. *J. Theor. Biol.* 223:93–111.

38. Sun, L., F. Yu, …, K. Machaca. 2011. Endoplasmic reticulum remodeling tunes IP_3-dependent $Ca^{2}+$ release sensitivity. *PLoS One.* 6:e27928.

39. Plotnikova1, O. V., E. N. Pugacheva, …, E. A. Golemis. 2010. Rapid calcium-dependent activation of Aurora-A kinase. *Nat. Commun.* 1:64.

40. Tombes, R. M., and G. G. Borisy. 1989. Intracellular free calcium and mitosis in mammalian cells: anaphase onset is calcium modulated, but is not triggered by a brief transient. *J. Cell Biol.* 109:627–636.

41. Rauh, N. R., A. Schmidt, …, T. U. Mayer. 2005. Calcium triggers exit from meiosis II by targeting the APC/C inhibitor XErp1 for degradation. *Nature.* 437:1048–1052.

42. Gerdes, H. H., and R. N. Carvalho. 2008. Intercellular transfer mediated by tunneling nanotubes. *Curr. Opin. Cell Biol.* 20:470–475.

43. Gurke, S., J. F. Barroso, …, H. H. Gerdes. 2008. Tunneling nanotube (TNT)-like structures facilitate a constitutive, actomyosin-dependent exchange of endocytic organelles between normal rat kidney cells. *Exp. Cell Res.* 314:3669–3683.

44. Önfelt, B., S. Nedvetzki, …, D. M. Davis. 2006. Structurally distinct membrane nanotubes between human macrophages support long-distance vesicular traffic or surfing of bacteria. *J. Immunol.* 177:8476–8483.

45. Nakagawa, S., S. Maeda, and T. Tsukihara. 2010. Structural and functional studies of gap junction channels. *Curr. Opin. Struct. Biol.* 20:423–430.

46. Nualart-Marti, A., C. Solsona, and R. D. Fields. 2013. Gap junction communication in myelinating glia. *Biochim. Biophys. Acta.* 1828:69–78.

47. Handly, L. N., and R. Wollman. 2017. Wound-induced Ca^{2+} wave propagates through a simple release and diffusion mechanism. *Mol. Biol. Cell.* 28:1457–1466.

48. Huo, B., X. L. Lu, …, X. E. Guo. 2010. An ATP-dependent mechanism mediates intercellular calcium signaling in bone cell network under single cell nanoindentation. *Cell Calcium.* 47:234–241.

49. Junkin, M., Y. Lu, …, P. K. Wong. 2013. Mechanically induced intercellular calcium communication in confined endothelial structures. *Biomaterials.* 34:2049–2056.

50. Slater, J. H., P. J. Boyce, …, W. Frey. 2015. Modulation of endothelial cell migration via manipulation of adhesion site growth using nanopatterned surfaces. *ACS Appl. Mater. Interfaces.* 7:4390–4400.

51. Doxzen, K., S. R. K. Vedula, …, C. T. Lim. 2013. Guidance of collective cell migration by substrate geometry. *Integr. Biol.* 5:1026–1035.

52. Thakar, R. G., Q. Cheng, …, S. Li. 2009. Cell-shape regulation of smooth muscle cell proliferation. *Biophys. J.* 96:3423–3432.

53. Tang, J., R. Peng, and J. Ding. 2010. The regulation of stem cell differentiation by cell-cell contact on micropatterned material surfaces. *Biomaterials.* 31:2470–2476.

54. Zhao, H., T. Li, …, X. Pan. 2019. AMPK-mediated activation of MCU stimulates mitochondrial Ca^{2+} entry to promote mitotic progression. *Nat. Cell Biol.* 21:476–486.

55. Rizzuto, R., D. De Stefani, …, C. Mammucari. 2012. Mitochondria as sensors and regulators of calcium signalling. *Nat. Rev. Mol. Cell Biol.* 13:566–578.

56. Santo-Domingo, J., and N. Demaurex. 2010. Calcium uptake mechanisms of mitochondria. *Biochim. Biophys. Acta.* 1797:901–912.